Experimental and numerical study of wavy mechanical face seals operating under pressure inversions

Jérémy Cochain, Noël Brunetière, Andrew Parry, Henri Denoix, Abdelghani Maoui

Article type:
Original article

Corresponding author info:
Jeremy Cochain, Institut Pprime, CNRS UPR3346, 11 Bd Marie et Pierre Curie, F-86962 Futuroscope Chasseneuil, France
Email : jeremy.cochain@univ-poitiers.fr

Article title:
Experimental and numerical study of wavy mechanical face seals operating under pressure inversions

Authors:
Jeremy Cochain[1*], Noël Brunetière[1], Andrew Parry[2], Henri Denoix[2], and Abdelghani Maoui[3]
1 Institut Pprime, CNRS UPR3346, 11 Bd Marie et Pierre Curie, F-86962 Futuroscope Chasseneuil, France
2 Schlumberger, 1 rue Becquerel, 92140 Clamart, France
3 CETIM, Technical Center of Mechanical Industry, 74 route de la Joneliere, 44000 Nantes, France

Abstract:
This paper investigates the impact of the face waviness and pressure inversions on the leakage and on the outer fluid entry of mechanical face seals using a numerical model and an experimental setup. The numerical model couples a transient Reynolds equation, an analytical contact model, a force balance solver, and a solver for the thermo-mechanical deformations. The experimental tests on a face seal with low waviness and on a face seal with high waviness provide leakage and outer fluid entry data, which are reproduced by the model.
Contrary to the face seal with low waviness, the face seal with high waviness has poor performance and the pressure inversions increase significantly the ingression of outer fluid. The parametric study shows a decrease of leakage with increasing spring force, and an increase of leakage and outer fluid entry with increasing values of waviness amplitude. The higher leakage observed for wavy seals is shown to be due to the higher average film thickness, and to some extent due to the mechanisms associated with waviness: hydrodynamic pressure generation, film squeeze and stretching.

Keywords:
Face seal, pressure inversion, waviness, seal dynamics, thermo-mechanical deformations, experimental, numerical, transient behaviour.

1. Introduction

Mechanical face seals are widely used in the industry to seal rotating shafts. They are composed of two rings in relative motion, one fixed to the stationary chassis, one fixed to the rotating shaft. The rings are pressed together using springs or bellows and their contact is lubricated by pressurised sealed fluid.
In some application [1, 2] face seals are subjected to pressure pulses and it is important to determine their impact on the performance, in particular when they lead to pressure inversions.
Similarly to the pressure pulses, the waviness of the faces lead to unsteady phenomena. The impact of pressure pulses and waviness on the performance of faces are the two aspects investigated in this paper.

The impact of varying pressure on the performance of mechanical face seals has only received limited attention. Harp and Salant in [3] presented a model to study the variation of the performance of an aerospace face seal during start-up and shut-downs, associated with pressure increase and decrease respectively. The model comprises a fluid, contact and deformation solvers in embedded loops. This study showed how the heat generation, contact force, and leakage vary over time for an inside or an outside pressurised seal and for a seal with a converging or diverging gap. The time scales of the unsteady processes studied are however of a few seconds and cannot be extended to smaller times scales. Paul and Salant in [4] studied an electronically-controlled seal under various conditions including step and oscillating pressure variation. The control of the seal is made by adjusting the coning of the carbon face using a piezoelectric actuator bonded to it. The feedback of the controller is based on the face temperature or leakage. The study demonstrated that the control system maintains the seal performance even when the pressure oscillates.

Face waviness correspond to deviation from flat in the circumferential direction. Such defect exists after manufacturing and change in operation due to the temperature gradients, drive elements or exposure to fluid pressure. Typical waviness for face seals after manufacturing and polishing ranges from 0.1 to 1 µm peak-to-peak with a length scale of 10 to 100 mm [5]. Minet et al. in [6] tested and measured three sets of face seals to provide some relevant statistical parameters for the surface, including waviness. The face seals were measured in their initial state, after a 24h-run in period, and worn after 124 hours testing. The authors observed that there are generally two waves on the faces and that the amplitude of the waves tend to increase with time, up to values close to 1 µm for the face seal tested.
In other experimental work on wavy face seals, such as in [7], Lubbinge tested face seals with a hard surface with waviness ranging from 0 to 5 µm. Flitney and Nau in [8] showed that after 100h test, the waviness of a carbon face reaches values ranging from 2 to 5 µm while the waviness of the hard face remains around 0.2 µm.
The effect of waviness was investigated by Lebeck in [9] who showed that they increase hydrodynamic load support but also lead to higher leakage. Some authors, such as Young and Lebeck in [10, 11], also designed face seals with deliberate waviness. These wavy-tilt-dam face seals have a waviness so chosen, as to enhance the load support and leakage control; while reducing friction and wear. The face seals were successfully tested under various test conditions, including high pressure, temperature, air ingestion and abrasives. Brunetiere et al. in [12] presented a parametric study of a mechanical face seal carried out with a numerical model considering thermo-elastic deformations. The variation of numerous input parameters was investigated including the waviness, with values up to 1.5 µm on the rotor. The simulations showed that, despite the circumferential variation of the film thickness, the global parameters are only negligibly affected by the waviness. In particular, the temperature rise only increase by 3 % with waviness. Ying et al. in [13] used a 3D model which includes thermo-elastic deformations to study the behavior of a wavy-tilt-dam seal under transient conditions, such as speed and pressure ramp.
The desirable hydrodynamic load support observed with waviness can also be obtained by machining notches on one of the faces. Mayer in [14] presented a thermohydrodynamic seal which is a mechanical face seal with notches. As shown in the article, the notches increase the load carrying capacity while reducing the friction coefficient. Such design allows to increase to operating limit a of given face seal. Djamai et al. in [15] presented a numerical model for a face seal with notches on one face. The model couples a fluid equation with cavitation, an energy, and deformation equations. Interestingly, the notches do not generate large hydrodynamic effects as the un-notched carbon face deforms thus leading to reduced film thickness variation in the circumferential direction. This deformation is due to fact that the film and face stiffness are of the same order of magnitude.
All these studies considered that only one of the faces has waviness. For seals with two hard surfaces, waviness is expected on both faces.

The present article investigates the effects of face waviness on the performance of mechanical face seals operating under pressure inversions.
Such an objective requires the development of a numerical model including a transient Reynolds equation, a contact model and a thermo-mechanical deformation module. A dedicated setup is also used to test the face seals and to provide experimental data.

2. Numerical model

The numerical model couples a transient Reynolds equation solver, an analytical contact model, an axial force balance

solver and a thermo-mechanical deformation solver.

2.1. Face seal configuration

The face seal is composed of a rotor and stator with a film of fluid lubricating the interface as shown on figure 1.

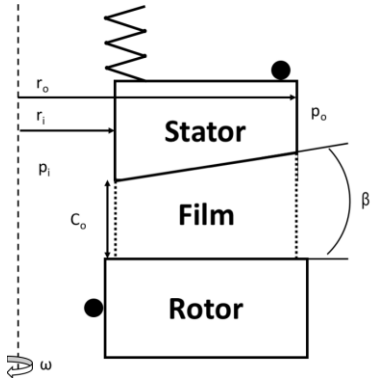

Figure 1: Schematic of a face seal. The distance between the centre of the faces is C_0, the pressures p_i, p_o; the radii r_i, r_o; and the rotating speed ω.

The surfaces of the rotor and of the stator are both considered with a 2-lobe waviness. The amplitude of the waviness is A_{wr} for the rotor and A_{ws} for the stator. The circumferential position in the reference frame is θ, and θ_r is the circumferential position of the rotor, which changes over time due to the rotation when observed in the reference frame. The film thickness, h, takes the form

$$h = A_{ws}\cos(2\,\theta) + A_{wr}\cos\big(2(\theta-\theta_r)\big) + C_0 + z(r) \qquad 1$$

Where C_0 is the central clearance and z is a term including initial radial defects of the faces as well as thermo-mechanical induces deformation. As can be seen, when both faces have waviness the film thickness changes over time.

2.2. Fluid film model

The transient Reynolds equation is

$$\frac{\partial}{\partial x}\left(\frac{\rho h^3}{\mu}\frac{\partial p}{\partial x}\right)+\frac{\partial}{\partial y}\left(\frac{\rho h^3}{\mu}\frac{\partial p}{\partial y}\right) = -6y\omega\frac{\partial}{\partial x}(\rho h) + 6x\omega\frac{\partial}{\partial y}(\rho h) + 12\frac{\partial}{\partial t}(\rho h) \qquad 2$$

where p is the fluid pressure, h the film thickness, μ the viscosity, ω the rotating speed, ρ the fluid density, and x and y the coordinates in the reference frame.

The model includes cavitation using the homogeneous approach of [16, 17]. The density of the mixture is given by

$$\rho = \frac{1}{\frac{1-\lambda}{\rho_l}+\frac{\lambda}{\rho_g}} \qquad 3$$

Where ρ_l and ρ_g are the lubricant and gas density, and λ the gas mass fraction, typically of 10^{-5} to 10^{-7}, and of 10^{-6} here. The gas density is given by the ideal gas law and thus varies with pressure and temperature whereas the liquid density is constant. The viscosity is determined using [18]

$$\mu = \frac{1}{\frac{1-\lambda}{\mu_l}+\frac{\lambda}{\mu_g}} \qquad 4$$

The viscosity of the gas and the viscosity of the liquid are supposed to depend on the temperature following

$$\mu_i(T) = \mu_i(T_0)\exp b_{visc\ i}(T-T_0) \qquad 5$$

Where i can be l or g depending on the media. b_{visc} is the coefficient of thermo-viscosity of the considered media, T the temperature, and T_0 a temperature at which the viscosity $\mu(T_0)$ is known.

The Reynolds equation is discretized using a finite element technique [17]. Since the density depends on the unknown pressure there is a convective term in pressure. An upwind scheme is necessary to avoid numerical oscillations, such procedure is known for gas lubrication [19,20] or cavitation modelling [21]. The transient term is treated with a first order

implicit Euler scheme.

Note that the effect of roughness is not considered in the Reynolds equation. Flow factors could have been used but their inability to capture important effects such as roughness induced pressure generation led the authors to not include them in the model.

2.3. Contact model

The model is based on the Greenwood and Williamson model [22] and assumes an exponential distribution of the peak heights, as done in e.g. [23]. The contact pressure is of the form

$$p_c(h) = \frac{E'}{8Sal} S_q \sqrt{\frac{\pi}{8}} \exp(1) \exp(-\frac{2h}{S_q}) \qquad 6$$

Where E' is the equivalent Young's modulus, *Sal* is the surface correlation length, and S_q the surface roughness standard deviation.

2.4. Axial force balance

The distance C_0 between of the faces is determined through the axial force balance applied to the floating element

$$-F_{spring} - F_{hydraulic} + F_{fluid} + F_{contact} = 0 \qquad 7$$

F_{spring} is constant. $F_{hydraulic}$ is given by $F_{hydraulic} = p_o BS + p_i(1-B)S$, with B the balance ratio and S the contact area. F_{fluid} and $F_{contact}$ are obtained from the pressure distributions obtained from of eq. 2 and eq. 6

$$F_{fluid} = \int_S p \; dS \qquad F_{contact} = \int_S p_c \; dS \qquad 8$$

The mass of the tested seal being small it has been neglected in equation 7. A post verification confirmed our assumption. The mass of the floating ring is and the maximum acceleration is. Their product is only **% of the closing force.
The initial guess of the face center distance is adjusted until the forces are equal using a Newton method. That is to say that a numerical derivative of the contact and fluid is calculated and used to update the seal clearance C_0.

2.5. Themo-mechanical deformation model

The fluid shearing and asperity contact generate heat that increases the film temperature and that diffuses to the faces. The increase of film temperature changes the viscosity henceforth the leakage. The diffusion of the temperature in the rotor and the stator leads to face deformations which change the shape of the interface. The thermal effects and thermo-mechanical deformations are therefore to be considered to correctly predict face seal performance. The thermal effects in the solids and thermo-mechanical deformations are considered axi-symmetrical.
The heat diffusion in the solids is given by

$$\rho C_P \frac{\partial T}{\partial t} - k\left(\frac{1}{r}\frac{\partial T}{\partial r} + \frac{\partial^2 T}{\partial r^2} + \frac{\partial^2 T}{\partial z^2}\right) = 0 \qquad 9$$

with C_P the heat capacity and k the thermal diffusion coefficient. The heat fluxes generated at the film level by the contact of the asperities, q_{dry}, and the shearing of the fluid, q_{visc}, are obtained by multiplying the shear stress by the surface velocity components:

$$\begin{aligned} q_{dry} &= f \; p_c \omega \sqrt{x^2 + y^2} \\ q_{visc} &= \omega(x\tau_{yx} - y\tau_{xz}) \end{aligned} \qquad 10$$

With f the friction coefficient between asperities and τ the viscous shear stress.
The heat is assumed to be transferred from the face seal rings to the environment by convection. The convective heat flow per unit surface is of the form

$$q = (T - T_\infty) h_c \qquad 11$$

With h_c the convection coefficient obtained using the Becker correlation [24]. The heat transfer equation is solved in the rotor and stator in one model. The film heat fluxes partition therefore automatically into the solids while ensuring that the rotor and stator faces have the same temperature. Since the model is axi-symmetrical, the circumferential average of q_{visc} and q_{dry} are considered at each radius.
Given that the film thickness is small, the temperature of the lubricant in the interface is set equal to the temperature of faces.
The thermo-mechanical deformations of the rings are given by (see e.g. [25])

$$\frac{E\nu}{(1+\nu)(1-2\nu)}\left[\frac{\partial^2 u_r}{\partial r^2}+\frac{\partial}{\partial r}\left(\frac{u_r}{r}\right)+\frac{\partial^2 u_r}{\partial r\partial z}\right]+\frac{E}{(1+\nu)}\left[\frac{\partial^2 u_r}{\partial r^2}+\frac{1}{r}\frac{\partial u_r}{\partial r}-\frac{u_r}{r^2}\right]+\frac{E}{2(1+\nu)}\left[\frac{\partial^2 u_r}{\partial z^2}+\frac{\partial^2 u_r}{\partial r\partial z}\right]-\frac{\alpha E}{(1-2\nu)}\frac{\partial T}{\partial r}=-\rho\omega^2 r \quad (12)$$

$$\frac{E\nu}{(1+\nu)(1-2\nu)}\left[\frac{\partial^2 u_r}{\partial z\partial r}+\frac{\partial}{\partial z}\left(\frac{u_r}{r}\right)+\frac{\partial^2 u_z}{\partial^2 z}\right]+\frac{E}{(1+\nu)}\frac{\partial^2 u_z}{\partial z^2}+\frac{E}{2(1+\nu)}\left[\frac{\partial^2 u_r}{\partial r\partial z}+\frac{\partial^2 u_z}{\partial r^2}+\frac{1}{r}\frac{\partial u_r}{\partial z}-\frac{1}{r}\frac{\partial u_r}{\partial r}\right]-\frac{\alpha E}{(1-2\nu)}\frac{\partial T}{\partial z}=0$$

With E the Young's modulus, ν the Poisson's ratio and α the thermal expansion coefficient. The thermo-mechanical deformations are solved for the rotor and stator separately. The displacements u_r and u_z at the interface are used to determine the deformation contribution to the film thickness.

2.6. Flowchart

Figure 2 shows the algorithm of the numerical model.

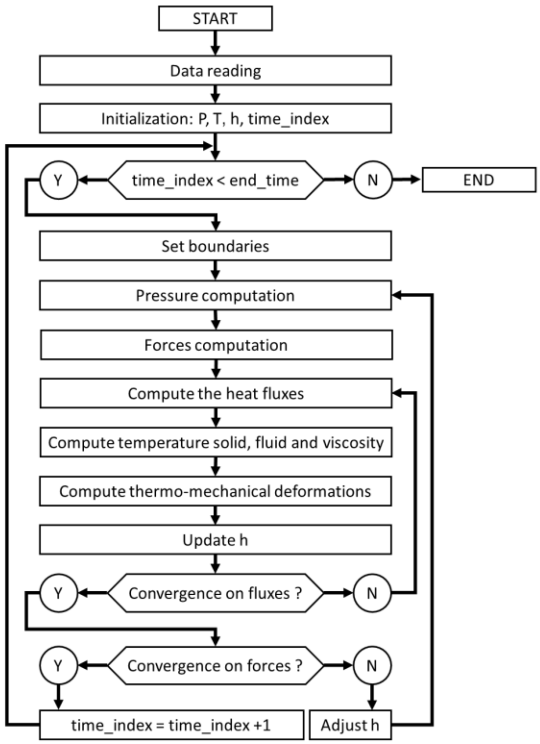

Figure 2: Numerical model workflow

The algorithm starts by reading the inputs and initialising the variables, including a guess on the film thickness. For each time step, the boundary conditions are set followed by a computation of the fluid pressure, forces, heat fluxes, temperature of the solids, temperature of the fluid, fluid viscosity and thermo-mechanical deformations. The initial film thickness guess is adjusted considering the forces and thermo-mechanical deformations. The loop for the thermo-mechanical deformations seeks convergence of the fluxes, the loop for the face distance seeks a convergence on the forces. Once convergence is reached on both loops, the algorithm moves to the next time step. The process is repeated for all time steps.

2.7. Comparison to published experimental results

The model is compared to the experimental results of [26] who made measurements of film temperature using infrared thermography for a contacting face seal with a sapphire stator. Figure 3 shows the film temperature increase at various radial positions and for various speeds.

The lines are the experimental data, the dots are the numerical predictions with a friction coefficient of 0.05 between the asperities. This coefficient was selected because the numerical predictions of the temperature are close to the experimental values at all speeds.

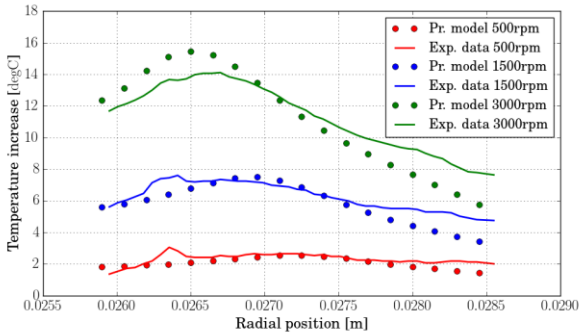

Figure 3: Comparison of the radial temperature increase for various speeds for the face seal of [26]. Experimental results: lines. Predictions of the present model: dots

One sees that the steady-state experimental temperature profile is well reproduced by the model. This comparison validates the model and give confidence in its predictions.

3. Experimental setup

3.1. Face seal of interest

The face seal, mounted onto the face seal holder, is presented on figure 4.

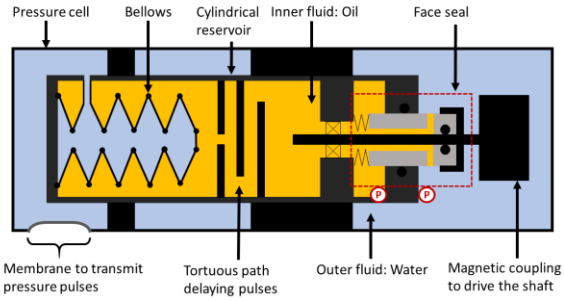

Figure 4: Face seal holder in the setup, immerged in water. The reservoir of lubricating oil in the face seal holder is slightly pressurized. The lubricant leaks through the face seal. The magnetic coupling rotates the shaft and rotor seal.

The face seal of interest is an outward face seal with lubricating oil at the inner radius and water at the outer radius. The stator is linked to the stationary part with springs and an O-ring. The rotor shaft is driven in rotation thanks to a magnetic coupling. The sides of the rotor and stator have flats to transmit/block the rotation. The rotor is blocked axially in the direction opposite to the stator.
The face seal holder is the mechanical system onto which the face seal is fitted.The functions of the face seal holder are to house the face seal, provide a reserve of lubricating oil and balance the pressure of the oil with the pressure of the water in the cell, while ensuring a small oil over-pressure of 1 to 2 bar.
As shown in figure 4, the main components of the face seal holder are: a cylindrical reservoir, a bellows, and a magnetic coupling connected to a shaft onto which the face seal is placed. The bellows is used to create the oil over-pressure and to compensate for the oil-loss. This experimental setup is the same as the one used in [27].

3.2. Pressure pulses

The pressure cell is connected to a pressure pulses generator (figure 4), the pulses are transmitted to the water of the pressure cell through membranes. The pressure pulses reach the outer radius of the face seal by travelling in water. The pressure pulses reach the inner radius of the face seal by travelling through the bellows and in the oil inside of the face seal holder. Due to the different nature of the acoustic paths, a pulse of pressure reaches the inner seal radius with a delay compared to the outer seal radius. An example of pressure reading and resulting pressure difference is shown on figure 5.

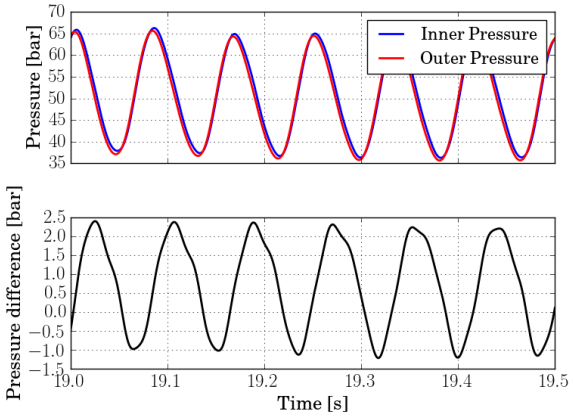

Figure 5: Inner and outer pressure measurements (top graph) and resulting pressure difference seen by the face seal (bottom graph).

The pressure pulses shown are +/- 15 bar at 12 Hz. (The signals are filtered with a low pass filter of cutting frequency 35 Hz). One sees that the inner pressure (blue curve) is lagging behind the outer pressure (red curve). The consequence of this delay is a varying pressure difference as shown in black.

Formally written, the pressures values are

$$p_i = p_{bp} + p_{\emptyset}$$
$$p_o(t) = p_{bp} + p_d \sin(2\ \pi f t) \qquad 13$$

With p_{bp} the back pressure, $p_{\emptyset}$ the over-pressure due to the bellow and p_d the pressure difference due to the delay.

3.3. Test conditions and test procedure

The test conditions are: temperature of 80°C; back pressure of 80 bar; bellow over-pressure of 1 bar, pressure pulses of +/-30 bar at 12 Hz leading to a pressure difference, p_d, equals to 3.55 bar. A rotating speed of 3500 rpm is set for 13 min and followed by 2 min without rotation. The pulses are generated when the shaft rotates. Typical test duration is 12h, plus a half day of assembly, and a half day of dissassembly.

The steps to carry out a test are as follow:

- Assembly of the face seal and face seal holder.
- Filling of the face seal holder with turbine oil following the creation of a vacuum. Collection of an oil sample and measure of the bellows compression.
- Insertion of the face seal holder in the setup, filling of the setup with water, increase of the pressure and temperature to the desired values.
- Starting of the test. The 12h tests ran overnight.
- Once the test is completed, setup cooling, decrease of pressure and removal of the face seal holder.
- Measure of the bellows compression. Emptying of the oil and collection of an oil sample.
- Shipment of the samples to an external lab.

3.4. Performance estimations

The performance of the face seal is characterized using:

- Variation of water in oil content
- Variation of oil volume

A sample of oil is collected during the filling of the face seal holder, before the test. At the end of the test, all the oil is collected, stirred and a representative sample taken. Both samples are sent to an external lab for analysis of water-in-oil content done with Karl Fisher titration [28].
The seal leakage is estimated by measuring the variation of the oil volume between the beginning and end of the test by inserting a rod into the bellows used to measure its length.

4. Results

This section presents the results of the experimental and numerical study on the impact of pressure inversions on the performance of wavy mechanical face seals.

Subsection 4.1 presents the face seal in nominal conditions and section 4.2 presents two simulations: One with a face seal without waviness and subjected to pressure pulses, one with a face seal with waviness with constant pressure. The objective is to observe the impact of each effect separately. The second subsection presents the experimental results and comparisons with the model with the objective of asserting the model prediction. The last subsection uses the model to carry out a parametric study on the impact of the waviness amplitude and closing force.

4.1. Face seal in nominal conditions

Figure 6 shows the model of the rotor and stator face considered. The configuration is axis-symmetrical for the thermo-mechanical deformations.

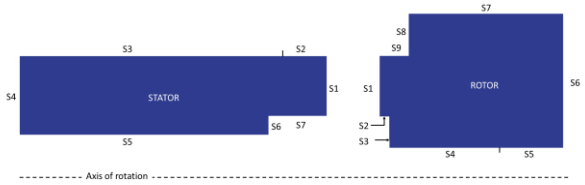

Figure 6: Model of the face seal

The contact surfaces are S1 on the rotor and stator. The surfaces in contact with lubricating oil or water are indicated in table 1 along with the mechanical and thermal boundary conditions.

Table 1: Boundary conditions of the model

	Stator		Rotor	
	Thermal	Mech.	Thermal	Mech.
S1	q_{var}	p_{var}	q_{var}	p_{var}
S2	$q_{conv,\ water}$	p_o	$q_{conv,\ oil}$	p_i
S3	$q = 0$	p_i	$q_{conv,\ oil}$	p_i
S4	$q_{conv,\ oil}$	p_i + z>=0	$q = 0$	p_i
S5	$q_{conv,\ oil}$	p_i	$q = 0$	p_o
S6	$q_{conv,\ oil}$	p_i	$q = 0$	p_o +z<=0
S7	$q_{conv,\ oil}$	p_i	$q = 0$	p_o
S8			$q_{conv,\ water}$	p_o
S9			$q_{conv,\ water}$	p_o

The convective heat flux per unit surface q_{conv} are given in equation 11.
The dimensions of the faces are presented in appendix. The lubricant properties in table 2, the material properties in table 3, the the operating condition in table 4 and the design parameter in table 5.

Table 2: Properties of the oil lubricant and water surrounding fluid at 80°C

Parameter	Unit	Value
Oil density	kg/m^3	962
Oil conductivity	W/K.m	0.14
Oil specific heat	J/kg.K	2000
Oil dynamic viscosity	Pa.s	0.0078
Oil Thermoviscosity coeff.	$10^{-6}/K$	-0.0243
$h_{c,oil}$	$W/K.m^2$	2013.6
Water density	kg/m^3	1000
Water specific heat	J/kg.K	4180
Water dynamic viscosity	mPa.s	0.355
$h_{c,water}$	$W/K.m^2$	22116.3

Table 3: Material properties of the silicon carbide rotor and stator

Parameter	Unit	Value
Density	kg/m^3	3170
Conductivity	W/K.m	150
Specific heat	J/kg.K	800
Young's modulus	GPa	434
Poisson's coefficient		0.21
Expansion coefficient	10^{-6}/K	3.70

Table 4: Nominal operating conditions

Parameter	Unit	Value
Rotating speed	Rpm	3500
Over-pressure $p_{\emptyset}$	bar	1.0
Surrounding fluid pressure p_b	bar	100
Temperature	°C	80

Table 5: Reference design parameter

Parameter	Unit	Value
Sq	µm	0.21
Sal	µm	1.78
Friction coefficient		0.1
Balance ratio B		1.0
Spring force	N	125

A simulation was performed with the data presented in tables 1 to 5. The performance of the face seal in these nominal conditions are shown in table 6. The dry and viscous friction torques of the seal is calculated in the following way:

$$C_{dry} = \int_S f \; p_c \sqrt{x^2 + y^2}\, dS \qquad 14$$

$$C_{visc} = \int_S (x\tau_{yx} - y\tau_{xz})\, dS$$

The mass flow rate $\dot{m}$ of the seal is calculated from the finite element formulation. The method is fully described in the appendix of paper [17].

Table 6: Performance of the face seal in nominal conditions

Parameter	Unit	Value
Leakage	cm^3/hr	0.137
Total torque	N.m	0.267
Dry torque	N.m	0.177
Viscous torque	N.m	0.090
Min. film thickness	µm	1.01
Max. film thickness	µm	1.09
Relative opening force due to contact	%	93.7
Dissipated power	W	97.7
Max. temperature increase	°C	9.3
Max contact pressure	bar	7.60

The face seal has a leakage of 0.137 cm^3/hr and a torque of 0.27 N.m which includes 0.177 N.m of dry torque (66%). The face seal exhibits a strong contact with close to 94% of the opening force supported by the asperities. The shape of the film thickness and the temperature increase distribution are shown on figure 7.

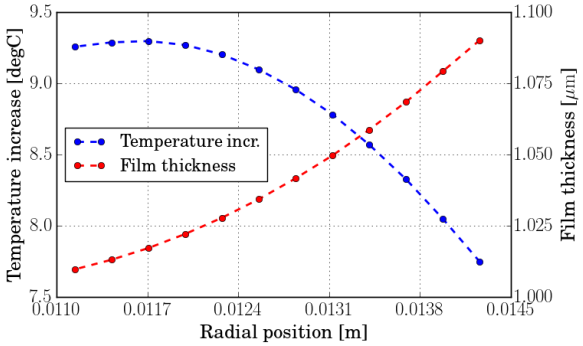

Figure 7: Radial film temperature and film thickness profiles of the face seal without waviness in nominal conditions.

Figure 7 shows that the faces of the seal form a diverging gap in the flow direction (inner to outer radius). The shape of the gap is due to the thermal deformations, and to the mechanical deformations to a lesser extend.

4.2. Effects of pressure inversions and waviness alone

4.2.1 Impact of pressure inversion

The reference simulation was performed over time and with the pressure pulses shown in equation 13. Figure 8 shows the variation of the average film thickness (black), of the mass flow at the inner (green) and outer (blue) radius resulting from the pressure pulses.

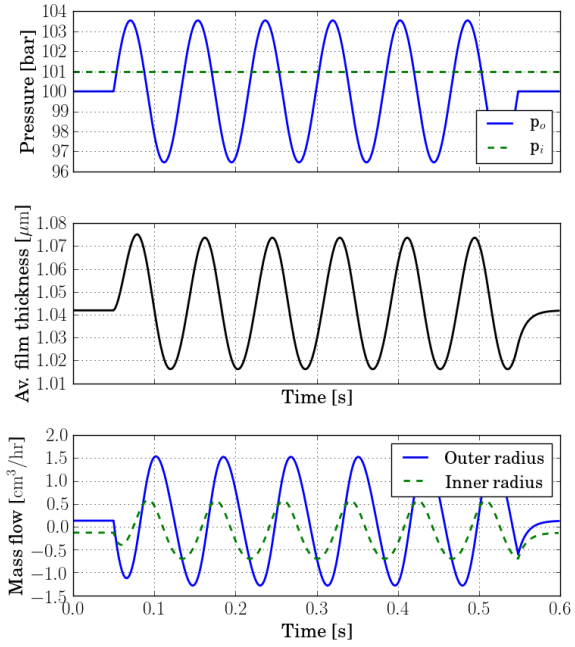

Figure 8: Time evolution of the pressures and resulting variation of the average film thickness and mass flows. Positive flow indicates fluid leaving the seal, negative entering.

Before the pulses start, that is, before time 0.05 s, the film thickness and mass flows are constant and equal 1.04 µm for the film thickness and 0.137 cm^3/hr for the mass flow (as presented in table 6). As the pressure varies, the film thickness and mass flows oscillate. The change of signs of the mass flow indicates that outer fluid water enters the sealing dam at the outer radius and that, at the inner radius, fluid in the sealing dam goes back to the sealed chamber. Water entering the seal, and potentially the sealed chamber, can be detrimental to the behavior of the seal and integrity of the surrounding systems.

The true value of water in the sealing dam is complex to estimate as it depends on numerous phenomena including surface wetting, water-oil mixing, etc.

The magnitude of water entry can be estimated by computing the cumulative of the circumferentially averaged massflow

$\dot{m}$ entering at the radii. The variables ζ_{ro}, ζ_{ri} are defined as

If $\zeta_{ro}(t^{j-1}) + \int_{t^{j-1}-\Delta t}^{t^{j-1}} \left(\frac{1}{\rho}\right) \dot{m}_{r_o}(t^j)dt < 0$ Then

$$\zeta_{ro}(t^j) = \zeta_{ro}(t^{j-1}) + \int_{t^{j-1}-\Delta t}^{t^{j-1}} \left(\frac{1}{\rho}\right) \dot{m}_{r_o}(t^j)dt \qquad 14$$

Else: $\zeta_{ro}(t^j) = 0$

If $\int_{t^{j-1}-\Delta t}^{t^{j-1}} \left(\frac{1}{\rho}\right) \dot{m}_{r_o}(t^j)dt > 0$ Then

$$\zeta_{ri}(t^j) = \zeta_{ri}(t^{j-1}) + \int_{t^{j-1}-\Delta t}^{t^{j-1}} \left(\frac{1}{\rho}\right) \dot{m}_{r_i}(t^j)dt \qquad 15$$

Else: $\zeta_{ri}(t^j) = 0$

ζ_{ro} increases over time if outer fluid enters the sealing dam at the outer radius; it decreases if the seal leaks as in nominal conditions but does not become negative. ζ_{ri} evolves in the same fashion but become null as soon as the fluid enters the seal at the inner radius (the inner reservoir of oil is supposed large so that the fluid entering it from the sealing dam is directly mixed with oil).

Figure 9 shows the evolution of the amount of water in the sealing dam ζ_{ro}/V (blue) and of the amount of sealed fluid of the sealing dam leaving ζ_{ri}/V (green).

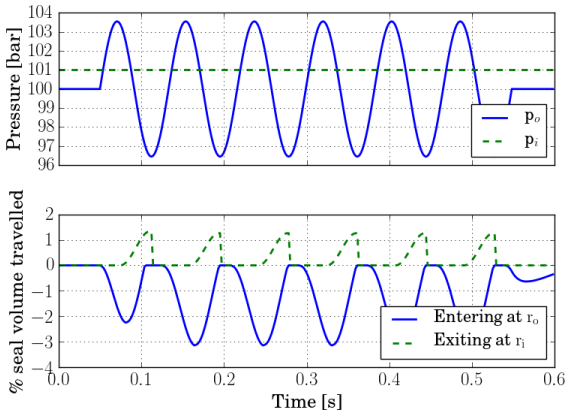

Figure 9: Time evolution of the pressures and resulting inflow of water at the outer radius, and outflow of sealed fluid at the inner radius expressed in percentage of total film volume.

One sees that, as the outer pressure becomes higher than the inner pressure, the water enters the seal at the outer radius. The water enters up to 3.1% of the total fluid volume and subsequently exist the sealing dam as the outer pressure becomes lower than the inner pressure. The amount of fluid leaving the seal at the inner radius correspond to a maximum of 1.3% of the total fluid volume in the film. Although the pressure reverses and the fluid at the outer radius temporarily enters the face seal, the duration of the pressure inversion is so short that the outer fluid does not travel more than a few percent of the total film volume.

This subsection showed that the pressure inversions lead to small amount of water entry. The values are small due to the low film thickness of the face seal studied, itself a consequence of the high spring force.

4.2.2 Impact of waviness

The primary objective is to understand the main effects caused by waviness. The waviness considered is based on surface topography measurements and is 0.4 µm for the stator and 0.5 µm for the rotor.

When a face seal has waviness on both faces, the film thickness distribution varies periodically. Figure 10 shows the relative position of the stator and rotor height at various time instants as the rotor rotates.

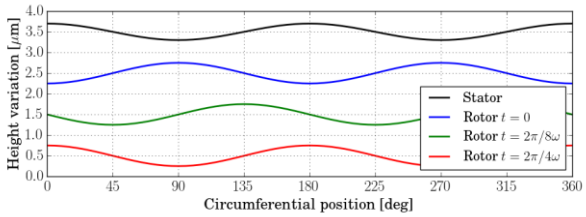

Figure 10: View of the positions of the rotor and stator lobes at various time instants.

In the initial configuration the rotor lobes face the stator lobe (blue and black curve). After ¼ of rotation the rotor lobes are between the stator lobe and valley and after another ¼ rotation (1/2 in total), the rotor lobes face the stator valley. The variation of mass flows, average and minimum film thickness are depicted on figure 11.

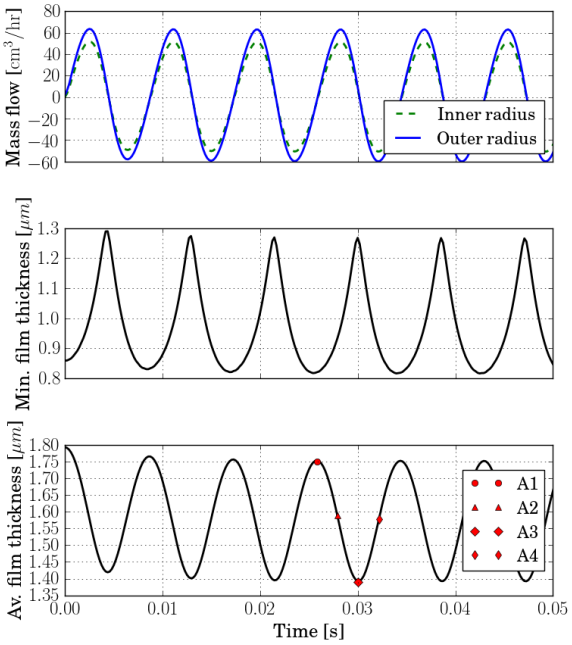

Champ de pression ici

Figure 11: Simulation of the face seal with low waviness. Time evolution of the mass flows, minimum film thickness, average film thickness (image of film volume) and snapshots of the fluid pressure distribution.

At time equals 0, the stator lobes face the lobe of the rotor, the minimum film thickness is the lowest and average film thickness highest. The pressure field is as shown on picture A1. As the rotor lobes move to stator valley, the minimum film thickness increases and average film thickness decreases (pressure field A2) until a lobe/valley configuration is reached (pressure field A3). The variables then return to the initial configuration and the pressure field passes through picture A4.
The average film thickness is an image of the seal volume. The variations of average film thickness lead to strong mass flow variations with entry of outer fluid at the outer radius and entry of film fluid at the inner radius, as shown on the top graph.
Aside from these overall variations of mass flows, there are local areas squeezed and stretched as shown on the pressure field A1 to A4. As such, the net mass flow at the inner and outer radius as shown on the top graph have contribution of fluid entering and leaving. This is illustrated on figure 12 for the flow at the outer radius.

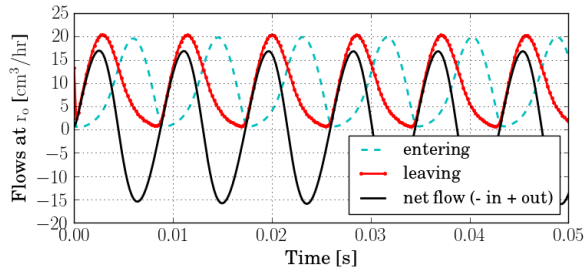

Figure 12: Mass flow entering and leaving the face seal at the outer radius. Face seal with low waviness.

The previously defined ζ_{ro}/V variable (equation 14) can be used to have an estimation of the water entry resulting from the waviness. Note that the variable is based on circumferential average of the mass flow at the outer radius and offer therefore only qualitative information. For the face seal with low waviness, the ratio ζ_{ro}/V, indicates that the water travels up to 10% of the total volume.
This is higher than with the pulses alone but not enough for the water to reach the oil reservoir.

4.3. Comparison to experimental results

This section compares the experimental results to the numerical predictions for face seals with two values of waviness amplitude. The face seal with low waviness has a waviness amplitude of 0.4 µm (0.8 µm peak-to-peak) on the stator and of 0.5 µm for the rotor. The face seal of high waviness has a waviness of 3.5 µm on the stator and 5.4 µm on the rotor.

4.3.1 Test results

The face seal with low waviness and a face seal prototype with the high value of waviness were tested on the setup. All tests are done at 80degC, 3500 rpm and with the pressure pulses indicated in equation 13. The test results are shown in table 7.

Table 7: Experimental test results with the face seal with low and high waviness amplitude and with or without pressure pulses

Test id	1	2	3	4	5
Waviness	Low	Low	High	High	High
Pulses	No	Yes	No	Yes	Yes
Duration, hours	12	12	3	3	5
State	Run-in	New	New	9h run-in	4h run-in
Vol loss cm^3/hr	< 0.8	< 0.8	126 +/- 3	85 +/- 3	78 +/- 2
Water in oil, before %	0.08	0.08	0.08	0.1	0.08
Water in oil, after %	0.13-0.19	0.3-0.32	0.39	3.14	5.5
Water in oil, incr. %	0.05-0.11	0.22-0.24	0.31	3.04	5.42
Water in oil, incr. rate %/h	0.0041 – 0.0092	0.018 – 0.02	.103	1.0	1.084

Face seals with low waviness ran for tests 1 and 2. It exhibits small values of water entry and a volume loss inferior to the measurement resolution. The values displayed are based on several tests. As can be seen by comparing the results of tests 2 and 1, the pressure pulses slightly increase the water content. These results show that the face seal with low waviness has excellent performance.

The face seal with high waviness ran for tests 3, 4, and 5. In contrast to the low waviness face seal, that seal exhibits large leakage, between 78 and 126 cm^3/hr, and large water ingression rate, between 0.1 to 1. percentage point per hour. These values are much higher that the acceptable standard limits.

None of the face seal tested showed visible marks of wear on the contact surfaces.

4.3.2 Simulation of the face seal with low waviness (0.4 µm – 0.5 µm) under pressure inversion

The face seal with low waviness used for tests 1 and 2 was simulated under the test conditions.
Figure 13 shows the resulting water entry expressed in percentage of total film volume travelled.

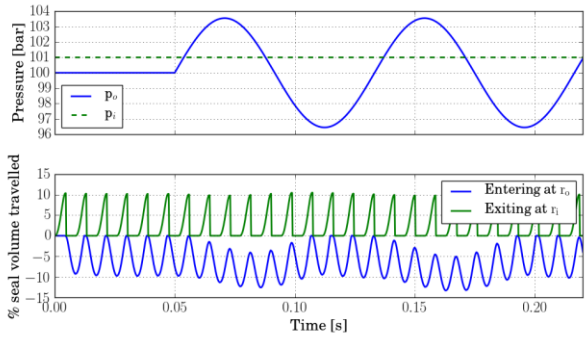

Figure 13: Time evolution of the pressures and resulting inflow of water at the outer radius, and outflow of sealed fluid at the inner radius expressed in percentage of the total film volume. Face seal with low waviness.

One sees that the maximum percentage of fluid volume travelled is 13.2%. This value is extremely close to the sum of the 10% due to the waviness alone and 3.1% due to the pulses alone shown in section 4.1. A maximum value of volume travelled of 13.2% is low, which is in accordance to the low values of water-in-oil obtained experimentally on tests 2.

4.3.3 Simulation of the face seal with high waviness (3.5 µm – 5.4 µm) under pressure inversion

The face seal with high waviness used for tests 3, 4, and 5 was simulated under the test conditions. The material properties of the face seal with high waviness, which are different from those of the face seal with low waviness, are given in table 8.

Table 8: Properties of the face seal with high waviness

Parameter	Unit	Value
Density	kg/m^3	3900
Conductivity	W/K.m	500
Specific heat	J/kg.K	500
Young's modulus	GPa	841
Poisson's coefficient		0.2
Expansion coefficient	10^{-6}/K	2.5
Sq	µm	0.368
λ	µm	7.1
Friction coefficient		0.08

Figure 14 shows the pressure boundary conditions, mass flow at the outer radius and percentage of seal volume travelled.

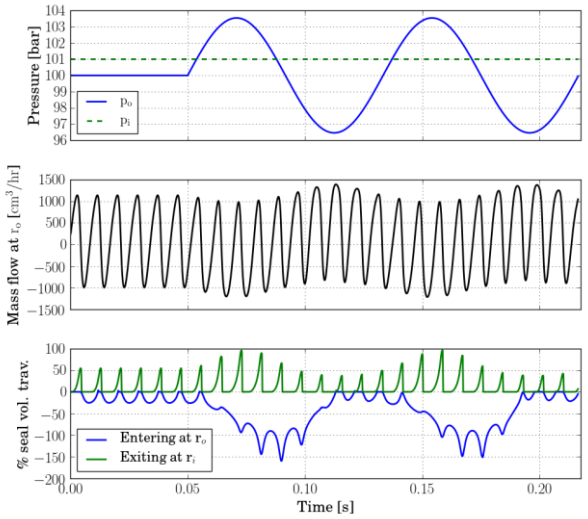

Figure 14: Time evolution of the pressures, resulting mass flow at the outer radius, inflow of water at the outer radius, and outflow of sealed fluid at the inner radius expressed in percentage of total film volume. Face seal with high waviness.

One sees that the mass flow varies between -1100 cm^3/hr to +1400 cm^3/hr which is more than one order of magnitude

than the reference face seal with waviness (see figure 11). When there are no pulses, that is, before time is 0.05 s, the water at the outer radius travels up to 25 % of the total volume, as a sole consequence of the waviness. The volume of fluid leaving the sealing dam at the inner radius to the oil reservoir is also high and equals 52% of the total sealing dam volume.
The distance travelled is much higher when there are pulses: the water at the outer radius travels up to 150% of the total fluid volume, the volume of fluid leaving the sealing dam at the inner radius to the oil reservoir is 100%. The high values obtained indicate water entry, which is in accordance to the high value of water-in-oil measured experimentally on tests 4 and 5. Further, the simulation indicates a leakage of 109 cm^3/hr.
The comparison between the experimental measurements and simulation results is presented in the next section.

4.3.4 Summary of the experimental and numerical comparisons

Table 9 summarises the experimental and numerical values of water entry obtained, while table 10 shows the results for the leakage.

Table 9: Comparison of the water entry predicted by the model and measured experimentally

Waviness	Low	Low	High	High
Pulse	Without	With	Without	With
Experiments, % / hr	0.004 – 0.0083	0.018-0.02	0.1	1.0
Simulation: Max(ζ_{ro}/V)	10%	13%	25 %	150%

Table 10: Comparison of the leakage predicted by the model and measured experimentally

Waviness	Low	Low	High	High
Pulse	Without	With	Without	With
Experiments cm^3 / hr	< 0.8	<0.8	126 ± 3	78 ± 2; 86 ± 3
Simulation cm^3 / hr	0.61	0.55	108.5	105.6

One sees that the model predictions are qualitatively aligned with the experimental measurements. These comparisons give confidence in the ability of the model to estimate water entry and leakage for wavy face seals. One also sees that the simulation predicts a lower leakage for face seals subject to pressure pulses as observed in the experiments.. The reason is due to the fact that the film thickness varies differently over time. To have a better view on the ability of the calculated volume travelled to detect water entry, it has been plotted as a function of the measured water entry rate in figure 15. It can be seen that a very good correlation exists between these parameters. Based on the fitted curve, it can be stated that if the calculated volume travelled is lower than 10%, no water entry is expected.
The next section presents a parametric study where the effect of waviness on the leakage as well as closing force is investigated.

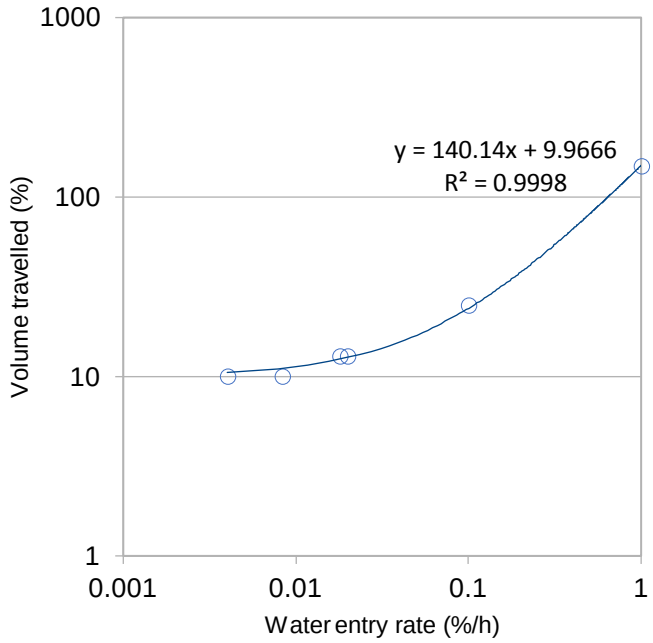

Figure 15: Calculated volume travelled as a function of the measured water entry rate .

4.4. Parametric study

This section investigates the impact of face waviness and closing force on the leakage and on the water entry.

4.4.1 Impact of the waviness on performance

The reference face seal is simulated with various realistic values of waviness. In this section the ratio of waviness defined as A_{ws} over A_{wr} (equation 2) is set at a constant value 0.8. The rotor waviness values A_{wr} (in µm) are: 0.3, 0.4, 0.7, and 1.0. The ratio of waviness is There are no pressure inversions for these simulations. Figure 15 shows the average leakage as a function of the average face waviness.

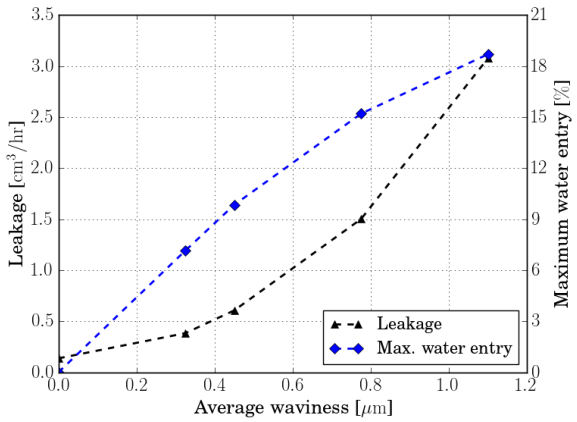

Figure 16: Impact of the average waviness on the leakage and maximum water entry.

The leakage of the case without flatness defect is 0.137 cm^3/hr (case of table 6). The leakage increases with increasing flatness defect and reaches up to 3.1 cm^3/hr with the maximum flatness defect simulated. This graph gives information on the maximum permissible waviness for a given leakage.

One sees that the maximum water entry increases when the flatness defect becomes higher.

4.4.2 Contributions to the leakage for wavy face seals

As seen on figures 8 and 11, the waviness of the faces increases the average film thickness. For face seals with parallel faces, the leakage is proportional to the cube of the film thickness. One wants to investigate if the higher leakage observed for wavy face seals is due to the increase of film thickness or to other effects.

A first set of simulations was performed on the face seal without waviness and with various values of Sq, each leading to a different value of film thickness. A second set of simulations was performed on the face seal with various values of waviness, each leading to a different value of film thickness. The leakage obtained are displayed as a function of the average film thickness in figure 16. For the simulations with wavy face seals, the time average over a period of the mean film thickness is considered.

The leakages are expressed in dimensionless form using

$$\hat{Q} = Q \ (6 \ \mu \ (r_o - r_i))/(\pi(p_i - p_o) r_{av} h_{av}^3) \qquad 16$$

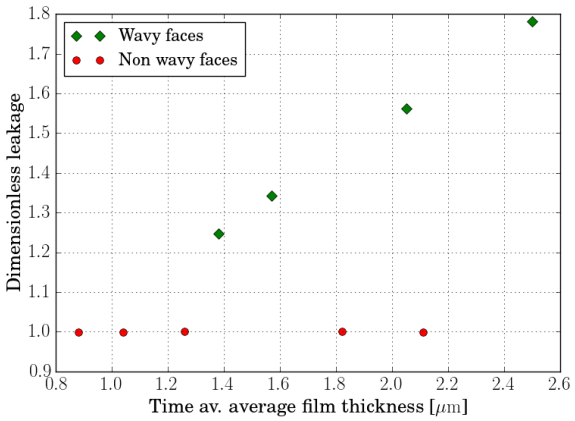

Figure 17: Comparative impact of the average film thickness due to face waviness and surface roughness on the leakage.

The red dots show the simulations with the non-wavy faces. The dimensionless leakage equals one is this case because it is driven by the Poisseuille flow. In contrast, the simulations with waviness have an increasing dimensionless leakage when the average film thickness is increased. This indicates that the leakage for wavy face seal is not only driven by the pressure difference but also by other mechanisms including hydrodynamic pressure generation, film squeeze and film stretching.

4.4.3 Impact of closing force for the face seal with low waviness

This section shows the impact of the closing force on the performance of the face seal with low waviness. Figure 17 shows the leakage and maximum water entry over the spring force for simulations without pulses (black) and with pulses (blue).

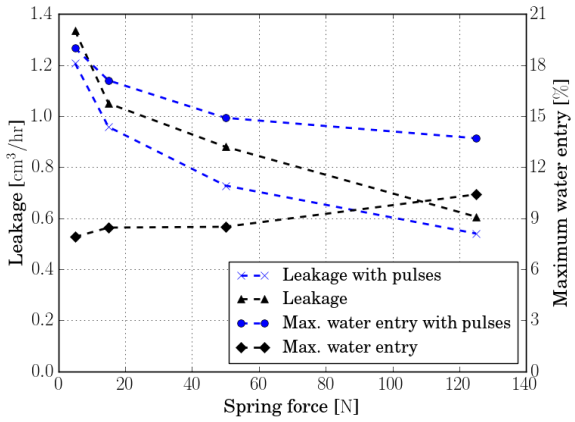

Figure 18: Impact of the spring force on the leakage and maximum water entry for a case with pulses (blue) and without pulses (black) for the face seal with low waviness.

One sees that the leakage decreases with the spring force with and without pressure pulses. This is due to the lower film thickness resulting from the higher contact force. As discussed previously, the leakage for the case with pressure pulses is slightly lower.
The maximum water entry decreases with the spring force for the case with pulses but slight increases without pulses. When the spring force is lower, the average film thickness is higher. This leads to lower squeeze and stretching effects, and therefore less propensity to water entry. In contrast, when the pressure reverses, the closing forces are not sufficient to compensate the reversing hydraulic force and the face seal tend to open which explains the higher water entry.

5. Conclusion

This article investigates, numerically and experimentally, the effects of pressure pulses on the performance, in terms of increase of leakage and potential outer fluid entry, of two wavy face seals.

A face seal with low waviness defect was experimentally tested under pressure inversions. The high contact force and low asperity height lead to a low film thickness which makes the seal have a low leakage and close to no water entry, despite operating in detrimental conditions.
An exploratory face seal with high waviness was tested under the same conditions and exhibits large leakage, some water entry with constant pressure, and significant water entry with pressure pulses. These results show the detrimental impact of waviness when coupled with pressure inversions.
The simulations of the face seals tested provided results in line with the experimental observations.

A numerical parametric study on the reference face seal shows that the waviness has a strong impact on the leakage (it varies from 0.137 to 3.1 cm^3/hr when the average waviness amplitude varies from 0.0 to 1.0 µm). This increased leakage is shown to be a consequence of the increased average film thickness and effects caused by waviness (hydrodynamic pressure, squeeze and stretching of the film). The propensity to water entry is also shown to increase with increasing waviness.
The parametric study on the reference face seal of low waviness showed that the leakage is increased when the spring force is reduced and that the propensity to water entry increases when there are pressure inversions due to unbalance of the hydraulic force by the spring force.

Nomenclature

A_{ws}, A_{wr}	amplitude of the waviness for the stator, rotor
B	balance ratio
b_{visc}	coefficient of thermo-viscosity
C_0	face centre distance
C_p	heat capacity
E	Young's modulus
F	force
h, h_{av}	film thickness
h_c	convection coefficient
p	pressure
q	heat flux per unit surface
r, z	cylindrical coordinates
r_i, r_o, r_{av}	radius
S	contact surface
S_q	standard deviation of surface roughness
t	time
T	temperature
u_r, u_z	deformations
V	film volume
x,y	cartesian coordinates in reference frame
θ	circumferential position
θ_r	rotor circumferential position
λ	gas mass fraction, thermal expansion coefficient, surface correlation length
μ	viscosity

ν	Poisson's ratio
ρ, ρ_l, ρ_g	mixture, liquid, gas density
β	radial taper
ω	rotational speed
ζ_{ro}, ζ_{ri}	amount of water entry

6. APPENDIX: Dimensions of the face seal

Table 11: Dimensions of the face seal

	Stator (mm)	Rotor (mm)
S1 inner radius	11.379	11.379
S1 outer radius	14.262	14.262
Length of S2	2.413	0.508
Length of S3	13.69	1.613
Length of S4	4.098	5.862
Length of S5	13.06	3.180
Length of S6	0.978	6.915
Length of S7	3.048	8.026
Length of S8		2.178
Length of S9		1.524

7. References

[1] Bur BH. Rock bit face seal having anti-rotation pins. Patent 6,176,330 B1, USA, 2001.
[2] Throp RE, Eason, EM and Borsos C. Pressure compensation and rotary seal system for measurement while drilling instrumentation. Patent 8,739,897 B2, USA, 2014.
[3] Harp SR and Salant RF. Analysis of mechanical seal behavior during transient operation. Journal of Tribology 1998; 120: 191-197.
[4] Paul JW and Salant RF. Electronically Controlled Mechanical Seal for Aerospace Applications—Part II: Transient Tests. Tribology Transactions 1995; 38: 51-56.
[5] Nau B S. Mechanical seal face materials. Proc. of the Institution of Mechanical Engineers, Part J: Journal of Engineering Tribology, 1997; 210: 165-183.
[6] Minet C, Brunetière N, Tournerie B and Fribourg D. Analysis and Modeling of the Topography of Mechanical Seal Faces. Tribology Transactions 2010; 53: 799-815.
[7] Lubbinge H. On the Lubrication of Mechanical Face Seals. PhD Thesis, University of Twente, Twente, The Netherlands, 1999.
[8] Flitney RK and Nau BS. A Study of Factors Affecting Mechanical Seal Performance. Proceedings of the Institution of Mechanical Engineers - Part A: Power and Process Engineering, 1987; 201: 17-28.
[9] Lebeck AO. Mechanical loading - a primary source of waviness in mechanical face seals. ASLE Transactions, 1997; 20: 195-208.
[10] Young LA and Lebeck AO. The design and testing of a wavy-tilt-dam mechanical face seal. Lubrication Engineering, 1997; 45: 322-329.
[11] Lebeck AO and Young LA. Wavy-tilt-dam seal ring, Patent 4836561 A, USA, 1987.
[12] Brunetière N, Tournerie B and Frêne J. TEHD Lubrication of Mechanical Face Seals in Stable Tracking Mode. Part 2 - Parametric Study. Journal of Tribology, 2003; 125:617-627.
[13] Ying L, Wei L, Yongjian L, Xiangfeng L, and Yuming W. Mechanism of a wavy-tilt-dam mechanical seal under different working conditions. Tribology International, 2015; 90:43-54.
[14] Mayer E. Thermohydrodynamics in mechanical seals. Fourth Int. Conference on Fluid Sealing, 1969: 124-129.
[15] Djamai A, Brunetière N, and Tournerie B. Numerical modeling of a thermohydrodynamic mechanical face seals. Tribology Transactions, 2010; 53:414-425.
[16] Brunetière N and Wang QJ. A simplified mass-conservating and continuous cavitation model. In 2011 STLE Annual Meeting and Exhibition, 2011.
[17] Brunetière N. A General Model for Liquid and Gas Lubrication, Including Cavitation. Journal of Tribology, 2018; 140:350-354.
[18] Saadat N and Flint WL. Expressions for the viscosity of liquid/vapour mixtures: Predicted and measured presure distributions in a hydrostatic bearing. IMechE, Part J, Journal of Engineering Tribology, 1996; 210:75-79.
[19] Bonneau D, Huitric J and Tournerie B. Finite Element Analysis of Grooved Gas Thrust Bearings and Grooved Gas Face Seals. ASME J. Tribol., 1993; 115: 348–354.
[20] Faria M. An Efficient Finite Element Procedure for Analysis of High-Speed Spiral Groove Gas Face Seals. ASME J. Tribol., 2001; 123: 205–210.
[21] Bonneau D and Hajjam D. Modelisation de la Rupture et de la Reformation des Film Lubrifiants Dans les Contacts Elastohydrodynamiques. Rev. Eur. Elem. Finis, 2001; 10:679–704.
[22] Greenwood J and Williamson JBP. Contact of nominally flat surfaces. Proc. Roy. Soc., 1966; 295: 300–318.
[23] Brunetière N and Tournerie B. Garnitures mécaniques d'étanchéité – Lubrification hydrodynamique et mixte Garnitures mécaniques d'étanchéité Lubrification hydrodynamique et mixte. Les Techniques de l'Ingénieur, 2016 (BM5422v1).
[24] Becker KM. Measurements of Convective Heat Transfer from a Horizontal Cylinder Rotating in a Pool of Water. International Journal of Heat and Mass Transfer, 1963:1053-1062.
[25] Salencon J. Mécanique des Milieux Continus - 1. Concepts Généraux. Ellipses, 1988.
[26] Adjemout M, Brunetière N, Bouyer J. Friction and temperature reduction in a mechanical face seal by a surface texturing: comparison between TEHD simulations and experiments. Tribology Transactions, 2018; 61 : 1084-1094.
[27] Cochain J. Numerical and experimental study of misaligned and wavy mechanical face seals operating under pressure pulses and inversions. PhD Thesis, University of Poitiers, France, 2018.
[28] Standard-NFISO6296: 2001. Dosage de l'eau - méthode de titrage Karl Fisher par potentionmétrie.